Available online at www.sciencedirect.com
ScienceDirect
Journal of the European Ceramic Society 31 (2011) 1549–1561
www.elsevier.com/locate/jeurceramsoc

Bone-like forming ability of apatite–wollastonite glass ceramic

M. Magallanes-Perdomo [a], Z.B. Luklinska [b], A.H. De Aza [a,*], R.G. Carrodeguas [a], S. De Aza [a], P. Pena [a]

[a] *Instituto de Cerámica y Vidrio (ICV-CSIC). C/Kelsen 5, Madrid-28049, Spain*
[b] *Queen Mary University of London, Materials Dept., London E1 4NS, United Kingdom*

Received 25 August 2010; received in revised form 25 February 2011; accepted 6 March 2011
Available online 8 April 2011

Abstract

This research describes the preparation, characterisation and *in vitro* behavior of a bioactive glass ceramic containing 44.8 wt% apatite, 28.0 wt% wollastonite-2 M and 27.2 wt% of amorphous phase. The biomaterial was obtained by a specific thermal cycle process that caused the devitrification of the $Ca_3(PO_4)_2$–$CaSiO_3$ binary system's stoichiometric eutectic composition. Overall, the material combines the properties of a resorbable Si–Ca-rich glass, in addition to bioactive properties of wollastonite and apatite phases. The bioactivity of this material was studied by soaking the samples in a simulated body fluid (SFB) for 3, 7, 14 and 21 days at 36.5 °C. During the soaking, the amorphous phase and also wollastonite-2 M phase underwent steady dissolution by releasing Si and Ca ions into the SBF medium. After 7 days, a porous hydroxy-carbonate apatite (HCA) layer was formed at the SBF–glass ceramic interface. The micro-nanostructured apatite–wollastonite-2 M glass ceramics with improved mechanical properties, in comparison with the parent glass, could serve as a promising platform for hard tissue regeneration.

Keywords: Simulated body fluid; Glass ceramics; Apatite; Wollastonite-2 M; Biomedical applications

1. Introduction

A series of calcium phosphate based biomaterials have been developed for hard tissue repair because of their excellent biocompatibility and osteoconductivity.[1–3] One of the most widely used synthetic calcium phosphate ceramics is hydroxyapatite (HA) due to its chemical similarity to the inorganic component of hard tisuses.[3]In the last two decades, calcium silicate based bioceramics have been studied as potential substitutes for hard tissue, because of their superior bioactivity compared to HA.[4] This property is attributed to the presence of silicon, which plays an essential role in the metabolic events that induce a new bone formation.[5–8]

Wollastonite-2 M and pseudowollastonite (low and high temperature forms of wollastonite, respectively) are the most common calcium silicate biomaterials proposed for bone tissue regeneration.[9] Major drawback of the $CaSiO_3$ bioceramics is their relatively fast dissolution rate that could comprise their mechanical strength. In addition, the pH of the surrounding medium significantly increases[10] which could affect the osseointegration of the substitute material within the natural bone.[11] The problem can potentially be solved by developing multiphase materials containing highly dissolvable phases like wollastonite on one hand and stable phases like HA on the other.

Kokubo et al.[12] were the first to develop A/W glass ceramic, composed of apatite and wollastonite crystalline phases in a glassy matrix. This bioceramic is highly bioactive and also mechanically strong in comparison to other glasses and glass-ceramics, because of wollastonite and apatite crystals' presence.[12]

The A/W glass-ceramic has been used in some medical applications, either in a powder form as bone filler or as a bulk material. These materials are currently manufactured by the powder processing methods, providing a uniform crystallisation of apatite and wollastonite phases in the glassy matrix, as the crystallisation of the parent glass in a bulk form leads to the appearance of large cracks.[13]

Other manufacturing methods have also been conducted in order to avoid milling the samples before the heat treatment application. Unfortunately, in some cases the final materials

* Corresponding author. Tel.: +34 91 735 58 64; fax: +34 91 735 58 43.
E-mail address: aaza@icv.csic.es (A.H. De Aza).

0955-2219/$ – see front matter © 2011 Elsevier Ltd. All rights reserved.
doi:10.1016/j.jeurceramsoc.2011.03.007

were non-bioactive when exposed to SBF.[14] In other cases, an additional crystalline phase, akermanite[15] was formed.

In our previous studies,[16,17] the mechanism of the crystallisation of the wollastonite ($CaSiO_3$, W)–tricalcium phosphate ($Ca_3(PO_4)_2$, TCP) eutectic glass was determined. In view of these findings, it was possible to design a series of heat treatment schedules and manufacture a wide range of bioglass ceramics containing various crystalline phases composed of phosphorous, silicon and calcium.

In this study, a specific heat treatment procedure is described, which allows manufacturing the glass ceramic composed of 44.8 wt% apatite, 28.0 wt% wollastonite-2 M and 27.2 wt% of an amorphous phase. As a starting material, the bulk eutectic glass composition was used, based on the W–TCP binary phase diagram.[18]

The bioactivity of the glass ceramic was assessed by immersion in a simulated body fluid (SBF) for 3, 7, 14, and 21 days. During the exposure to SBF, the solutions were examined for changes in Ca, Si, and P ions' concentrations, using inductively coupled plasma atomic emission spectroscopy (ICP-AES). The pH fluctuations of the SBF solutions were also recorded.

The morphological and chemical changes, which took place on the surfaces of the specimens and within the specimens, were examined by scanning (SEM) and transmission electron microscopy (TEM) methods, including energy dispersive X-ray spectroscopy (EDS).

2. Materials and methods

The binary system W–TCP shows a eutectic invariant point at $1402 \pm 2\,^{\circ}C$.[18] In the present work, a glass with eutectic composition corresponding to 60 wt% W–40 wt% TCP was chosen, as it represents the lowest melting temperature composition of the system.[18]

The chemicals used for the synthesis of the eutectic glass were reagent-grade calcium carbonate ($CaCO_3$, Merck, Darmstadt, Germany), high-purity amorphous silica (99.7 wt%, Strem Chemicals, USA) and high-purity synthetic $Ca_3(PO_4)_2$, which characteristics were reported previously.[17]

The mixed powders were melted for 30 min in a Pt-10 wt% Rh crucible at 1600 °C. This process allowed obtaining a fused material with sufficiently low viscosity to be poured out onto a warm metal plate, avoiding at the same time any possibility of devitrification. Next, taking into account the dilatometric data[17] the glassy block was annealed at 795 °C and then slowly cooled down to room temperature in order to eliminate the stress formed during the cooling process.

2.1. Apatite–wollastonite glass ceramic preparation

Apatite–wollastonite 2 M glass ceramic was obtained from the bulk eutectic glass composition through an appropriate thermal treatment of the eutectic composition of the W–TCP binary system.

In previous research,[16,17] the range of temperatures to produce a glass ceramics containing apatite–wollastonite 2 M phases was established. Based on this information, the eutectic glass was treated at 820 °C for 2 h, heated up to 1100 °C for 1 h and then cooled to room temperature at $5\,^{\circ}C\,min^{-1}$.

The final specimens were cut into pieces of $\sim$1.6 mm × 5.7 mm × 8.6 mm dimensions using low speed saw (Buehler, Lake Bluff, IL).

2.2. Characterisation of the apatite–wollastonite glass ceramic and parent glass

2.2.1. Phase identification and quantitative analysis

Glass and glass ceramic samples were characterised by powder X-ray diffraction (XRD) at room temperature. The samples were ground to powder with an average size below 63 μm and XRD patterns were recorded on a Siemens D5000 automated diffractometer (Karlsruhe, Germany) using $CuK_{\alpha 1,2}$ radiation (1.5418 Å) and a secondary curved graphite monochromator. Data were collected in the Bragg–Brentano ($\theta/2\theta$) vertical geometry (flat reflection mode) between 2° and 70° (2θ) in 0.05° steps, counting for 5 s per step.

The quantitative analysis of the phases present in the glass ceramic (including the amorphous content) was performed by the Rietveld method.[19] Therefore, the sample was milled and then mixed with CaF_2 as internal standard. The final mixture contained 70.0 wt% glass-ceramic and 30.0 wt% CaF_2. The analysed pattern was recorded in a more precise way (0.03° steps, counting 20 s per step).

All samples were rotated at $0.25\,s^{-1}$ during acquisition of patterns in order to improve powder averaging, which is essential with a view to obtaining accurate intensities and hence phase analyses. The diffractometer optic was a system of primary Soller foils between the X-ray tube and the fixed aperture slit. One scattered radiation slit of 1 mm (2 mm for Rietveld analyses) was placed behind the sample, followed by a system of secondary Soller slits and a detector slit of 0.1 mm (0.2 mm for Rietveld analyses). The X-ray tube was operated at 40 kV at 30 mA. The EVA-version 6.0 Diffrac plus software (Bruker AXS GmbH, Karlsruhe, Germany) was used to evaluate the patterns and GSAS (General Structure Analysis System) suite program[20] was used to refine the powder pattern.

2.2.2. Microstructural studies

The microstructure of the glass and glass ceramic samples were studied via field emission scanning electron microscopy (SEM, Hitachi-S4700, Tokyo, Japan). Additional studies were carried out by transmission electron microscopy (TEM, Jeol Jem 2010 at 200 keV, fitted with LaB6 filament).

For examination on the SEM, the glass ceramic samples were mounted in an epoxy resin and polished down to 1 μm grade. A cerium suspension was used in the final preparation, whenever appropriate. Samples were chemically etched with 5 vol.% acetic acid for 1 s.

The samples for the TEM were initially prethinned and then attached to the 3 mm TEM hole grids for final ion beam thinning on Precision Ion Polishing System, (Gatan Inc, USA), until a small perforation developed, using 5 kV argon ion beam. The thin sections were then coated with a thin layer of carbon and observed in TEM.

2.2.3. Chemical analysis

The eutectic glass ceramic was analyzed by X-ray fluorescence analysis (XRF) to verify the stoichiometric eutectic composition of the sample. A MagiX Super Q Version 3.0 Phillips X-ray fluorescence spectrometer (Philips, Netherlands) was used. This spectrometer is equipped with IQ+ analytical software used for qualitative and semiquantitative analysis. Calibration curves were fitted from the certified standards consisted of natural and synthetic calcium phosphates and calcium silicates.

For X-ray fluorescence analysis, the glass ceramic samples and standards were prepared as glass beads by lithium tetraborate fusion in a Perl'x2 machine (Philips, Netherlands). The powdered sample (0.3 g) and the flux (5.5 g of $Li_2B_4O_7$) were mixed and heated in a Pt-5 wt% Au crucible at 1100 °C. The molten mixture was cast as amorphous glass bead suitable for analysis.

2.3. Properties of the apatite–wollastonite glass ceramic

2.3.1. Bioactivity in static simulated body fluid (in vitro test)

The static simulated body fluid *in vitro* test was carried out by the procedure established by Kokubo in 1991.[21] In this work, a corrected SBF solution was used, which contained similar quantity of SO_4^{2-} ions as human blood plasma.

Samples of the glass ceramic were placed onto a plastic support and then in a plastic bottle containing calculated volume of SBF, following Eq. (1):

$$V_s = \frac{S_a}{10} \quad (1)$$

where V_s is the volume of SBF (ml) and S_a is the apparent surface area of specimen (mm^2).

The samples were then immersed in SBF and kept at 36.5 °C in the incubator for different periods of time (3, 7, 14 and 21 days).

After the exposure to the SBF, the microstructure of the surfaces and cross sections were studied by scanning electron microscopy using a Hitachi-S4700 (Tokyo, Japan) fitted with energy dispersive X-ray spectrometer. To study the cross sections of the samples these were cut with the previous mentioned low speed saw and then embedded in epoxy resin under vacuum. The samples were polished down to 1 μm diamond paste and carbon coated for SEM examination and EDS-microanalysis. Further, the products of the surface reaction were carefully removed using a razor blade and powdered in an agate mortar using alcohol and then placed on a carbon coated copper TEM grids for characterisation by TEM.

The changes in the concentration of Ca, Si and P ions in the SBF solutions were examined using inductively coupled plasma atomic emission spectroscopy (ICP-AES, Jarrel Ash Iris Advantage) (California, USA), while the pH fluctuations of the SBF solutions were also recorded using an ion-sensitive field effect transistor Hanna-HI4212 (Bedfordshire, UK).

To support the reaction mechanism between wollastonite-2 M ($CaSiO_3$) and SBF, thermodynamic calculations were performed using the HSC computation package (HSC Chemistry®)[22] that offers an exhaustive thermochemical database that includes enthalpy (H), entropy (S) and heat capacity (C) data for chemical compounds.

3. Results

3.1. Glass

The eutectic composition was completely melted at 1600 °C after 30 min and the melt was easily cast, resulting in a homogeneous, transparent and colourless glass. Neither cracks nor other defects were detected in the glass samples.

3.1.1. XRD and TEM analyses

The 795 °C/19 min annealed stress-free glass was amorphous with no crystalline phases present, as confirmed by X-ray diffraction (Fig. 1A). The amorphous XRD pattern registered only one broad peak (centre: *ca.* 30°, 2θ), which is a characteristic feature of alkaline earth silicophosphate glasses.[23–26,14]

Any evidence of phase separation or crystalline nuclei presence was examined by high resolution TEM method (Fig. 1B and C).

3.2. Glass-ceramic

X-ray fluorescence chemical analysis (Table 1) showed that the glass ceramic samples retained the stoichiometric eutectic composition, with no loss of any volatile component and that the level of the impurities was negligible.

3.2.1. XRD–Rietveld analysis

The XRD powder pattern of the glass ceramic (Fig. 2) showed the presence of apatite and wollastonite-2 M. The pattern was evaluated by Rieltveld method using the GSAS program. The crystal structure used to fit the apatite phase was previously reported by R.M. Wilson as $Ca_{9.303}(PO_4)_6(OH)_{0.606}1.97(H_2O)$,[27,28] whereas data for wol-

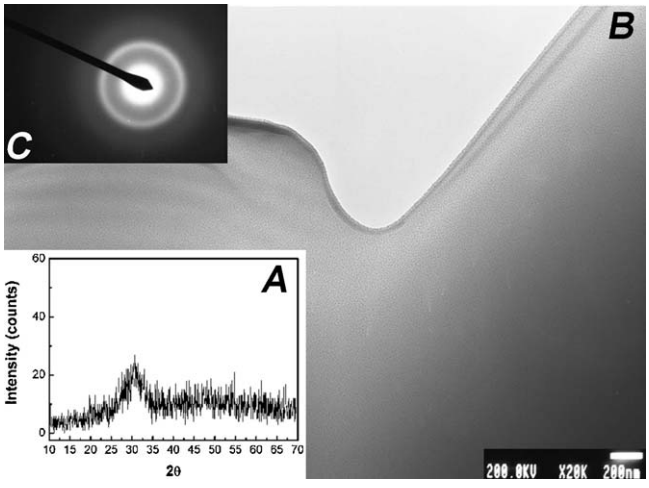

Fig. 1. (A) X-ray diffraction pattern of the glass after annealing. (B) Transmission electron microscopy micrograph and (C) SAD of the glass after annealing.

Table 1
X-ray fluorescence analysis of the eutectic W–TCP glass ceramic.

W–TCP	CaO	SiO_2	P_2O_5	MgO	Na_2O	K_2O	Fe_2O_3	MnO	TiO_2
Glass-ceramic	50.7(1)	30.7(3)	18.5(2)	0.10(1)	0.054(2)	0.001(3)	0.036(3)	0.005(1)	0.012(3)
Theoretical	50.7	31.0	18.3	–	–	–	–	–	–

The uncertainties of the last digit are given in parentheses.

Table 2
Phase composition and lattice parameters for the crystalline phases. Results obtained by Rietveld quantitative amorphous content analysis (RQACA).

	%wt.	Lattice parameters					
		a	*b*	*c*	alpha	beta	gamma
Apatite	44.8(7)	9.452(6)	9.452(6)	6.960(7)	90	90	120
Wollastonite	28.0(8)	15.428(4)	7.330(6)	7.051(9)	90	95.394	90
Amorphous	27.2(5)	–	–	–	–	–	–

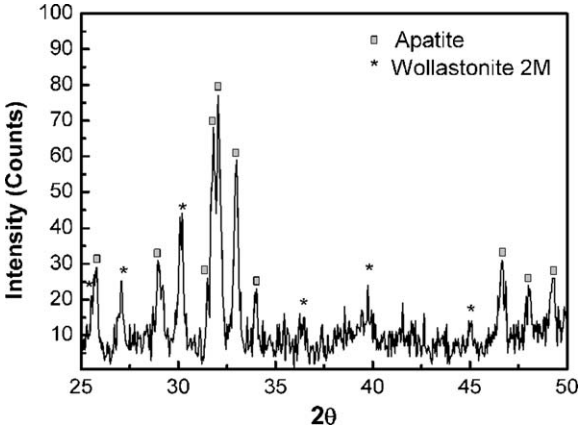

Fig. 2. X-ray diffraction pattern of the glass ceramic.

lastonite was reported by F. Jr. Trojer as $Ca(SiO_3)$.[29,30] The calculated fit parameters (R_{wp} and R_F) were less than 10%, indicating good and reliable match.[31] The results of the Rietveld quantitative amorphous content analysis (RQACA) are summarised in Table 2.

3.2.2. SEM and TEM studies

The microstructure of the glass ceramic as examined by SEM/EDS is shown in Fig. 3. The sample after chemical etching (Fig. 3A), disclosed microstructure features of micron to submicron size. The material was dense, homogeneous and composed of domains of around 2 μm in diameter, formed by a continuous interlocked residual calcium silicon phosphate amorphous phase (light gray phase) that encloses a homogeneous mixture of apatite (the dissolved phase by the chemical etching) and wollastonite-2 M crystals in the range of ∼20–50 nm in diameter (Fig. 3B).

Fig. 4 shows a transmission electron micrograph of the glass ceramic. Three different regions were distinguished. Selected area diffraction (SAD) patterns indicated that these regions were mainly composed of glass (Zone 1), apatite (Zone 2) and wollastonite-2 M (Zone 3). The latter phase showed a typical fibrous shape.

A magnified image of Zone 3 (Fig. 4) is presented in Fig. 5. This region contains nano-crystals of apatite and wollastonite-2 M of oval shape, in the range of about 20–50 nm in length and 20 nm in diameter. The wollastonite particles display twin contrast,[32] demonstrated by the banding of different spacing as shown in Fig. 5C (inside the black circle).

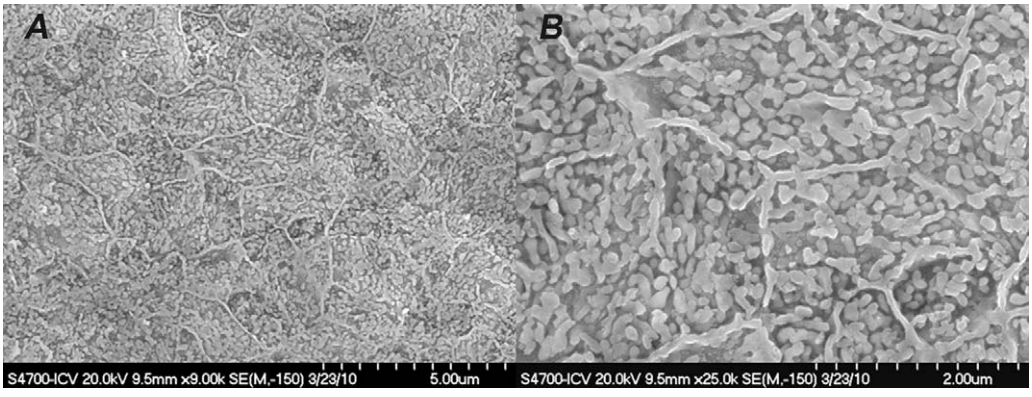

Fig. 3. Polished and chemically etched surface of the glass ceramic. Sample fired at 820 °C for 2 h, and then heated up to 1100 °C for 1 h. This sample presents a homogeneous microstructure formed by nanocrystals of apatite, wollastonite-2 M and a residual amorphous phase.

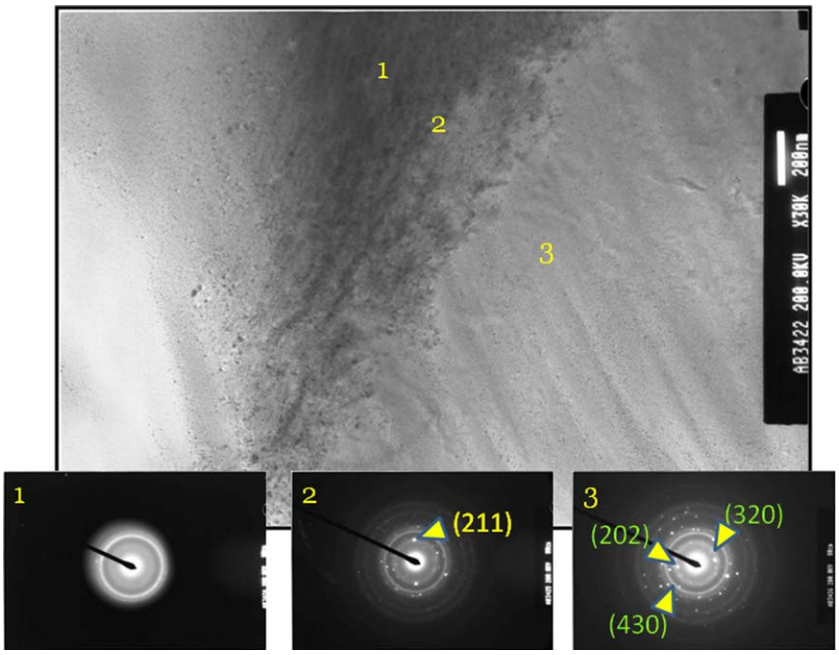

Fig. 4. Transmission electron micrograph of the glass ceramic. Zone 1: amorphous phase, Zone 2: apatite phase, Zone 3: mainly wollastonite-2 M phase.

3.2.3. In vitro bioactivity studies

The experimental variation in calcium, silicon and phosphorus ions concentrations in the SBF at 36.5 °C after the glass ceramic samples were soaked over 21 days period is presented in Fig. 6. The initial concentration of the SBF solution is also included for comparison.

The pH within the average SBF solution increased from 7.40 ± 0.02 to 7.50 ± 0.05 after 3 days exposure and remained almost constant during the rest of the monitoring period of 3 weeks.

SEM micrographs and EDS-microanalysis of the specimens' surface after the immersion for different periods of time in SBF are shown in Fig. 7. Fig. 7A–D presents EDS microanalysis taken from surfaces of the samples soaked for 3, 7, 14 and 21 days in SBF solution. The visible cracks displayed in some images are artifacts caused by the drying process of the specimen in air.

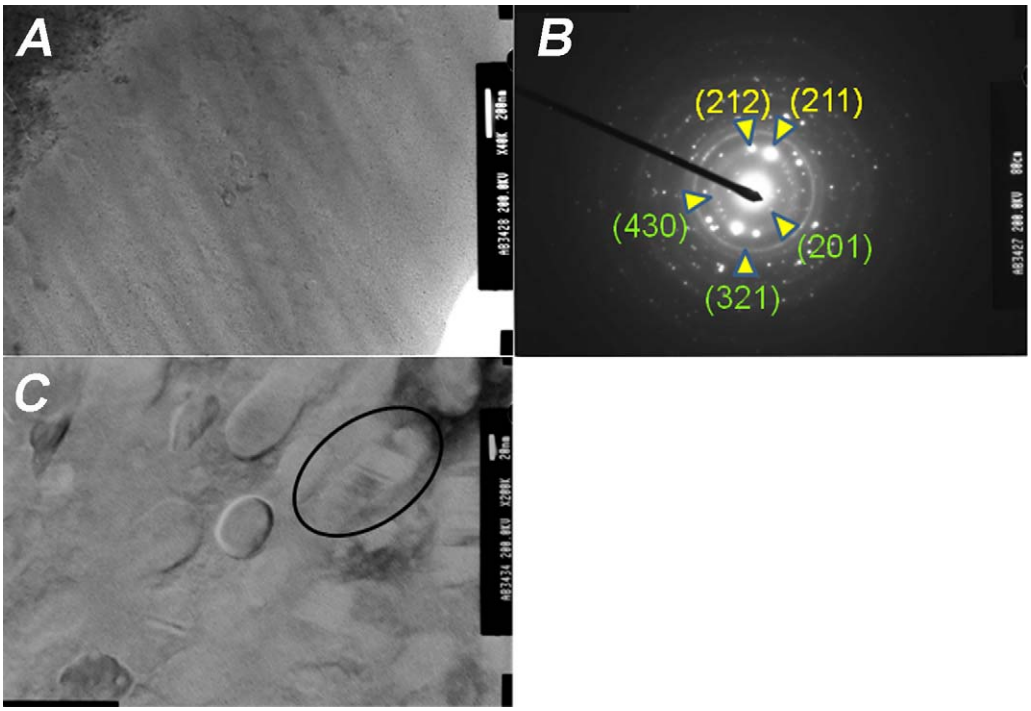

Fig. 5. (A) Detail of Zone 3 of Fig. 4. (B) SAD. (C) Magnified image of Zone A, showing nearly ellipsoidal nanocrystals of apatite and wollastonite-2 M and the latter phase displaying twin contrast.

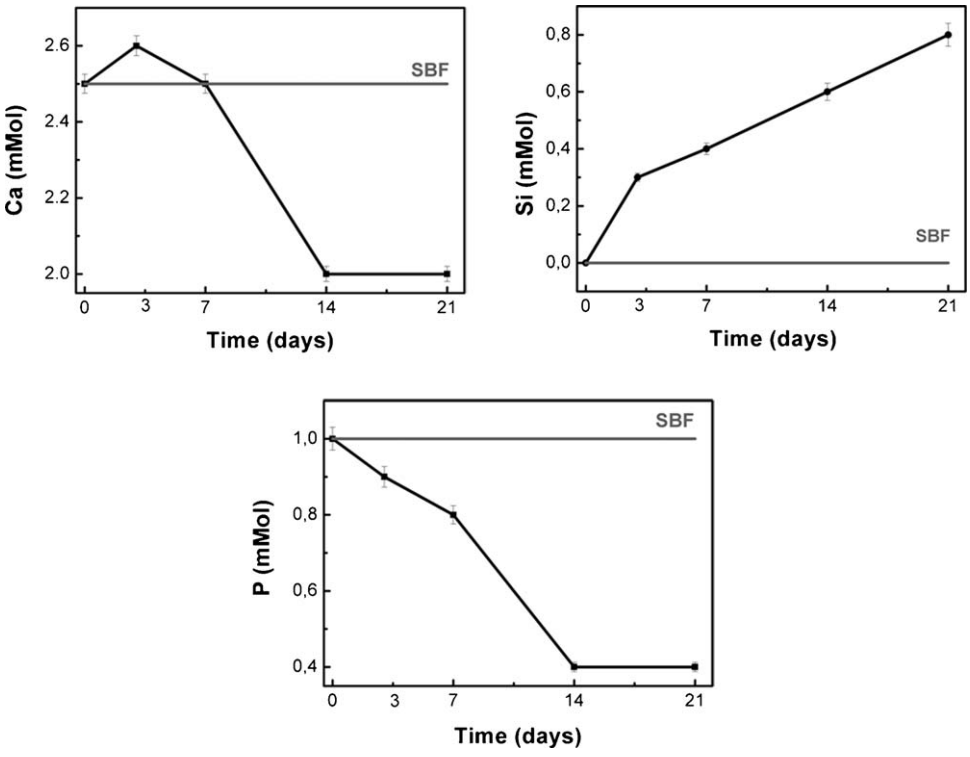

Fig. 6. Changes in calcium (Ca), phosphorus (P) and silicon (Si) ion concentration with soaking time in SBF during *in vitro* test. The line denoted as SBF, represents the initial value.

The Fig. 7A showed a selective dissolution, mainly of the continuous interlocked residual amorphous phase at the grain boundaries after 3 days in SBF. A discontinuous layer with some nano-size aggregates of the bone-like apatite and pores, formed on the surface after 7 days of soaking in SBF, is shown in Fig. 7B.

A continuous layer covering the surface of the sample was observed after 14 and 21 days of soaking, Fig. 7C and D. This layer was composed of crystals with plate-like morphology, which grain size increased with the immersion time. The SEM/EDS microanalysis showed that the newly formed apatite layer contained mainly Ca, P and small amount of Si (Fig. 7C and D), with a Ca/P ratio $\approx 1.66 \pm 0.03$ after 21 days of soaking. Also, some Mg, K and Na elements coming from the SBF were detected in the EDS spectra.

The SEM micrographs of the cross sections of the glass ceramic specimens, after soaking for 3, 7, 14 and 21 days at 36.5 °C in SBF revealed the microstructure of the glass ceramic/SBF interfaces (Fig. 8A–D). Fig. 8A and B shows a porous layer of reaction products developed after 3 and 7 days of soaking, respectively. The Zone 1, about 10 μm thick, of the sample immersed for 3 days in SBF (Fig. 8A) was composed on average of 28.90 at% Si, 20.81 at% P, 50.29 at% Ca, and had Ca and Si quantities lower than the original specimen (30.76 at% Si, 15.39 at% P, 53.85 at% Ca). A similar trend was observed in the sample soaked for 7 days; however, the reaction Zone 1 was significantly thicker, measuring about 15 μm (Fig. 8B).

For the specimens soaked in SBF for 14 and 21 days, the microstructural study revealed the formation of two well-defined successive layers at the interface. A massive formation of a new hydroxy-carbonate apatite (HCA) layer was observed at the SBF interface with the sample (Ca/P = 1.66–1.68). Adjacent to the HCA layer a porous structure developed parallel to the interface (20.98 at% Si, 28.47 at% P, 50.55 at% Ca), which formed by dissolution of the wollastonite-2 M grains and the continuous interlocked residual amorphous phase (Fig. 8C and D).

Overall, the microstructures revealed the formation of successive reaction layers at the SBF interface. Changes in the elemental concentration observed across the glass ceramic–SBF interface are shown in Fig. 9.

It was found that the porous reaction layer increased up to about 15 μm thickness within the first 7 days of exposure to SBF, while the HCA layer reached about 4 μm thickness after 21 days Fig. 10.

TEM microscopy was used to examine the ultrastructure of the surface product formed after soaking of the glass ceramic in SBF (Fig. 11). The results showed the presence of nanocrystals with a plate-like morphology, mainly composed of Ca and P. In addition, amorphous silica was identified in a specimen exposed to SBF for 7 days (Fig. 12).

4. Discussion

The parent glass obtained after the annealing treatment was free of any crystalline phase, as observed by TEM (Fig. 1B and C). This result agrees with the average pattern obtained from XRD (Fig. 1A), which showed the presence of amorphous material.The glass ceramic obtained from the parent glass contained ~72.8 wt% of crystalline phases, composed of apatite (44.8(7) wt%) and wollastonite-2 M (28.0(8) wt%), Table 2, hence the apatite constituted the main phase in

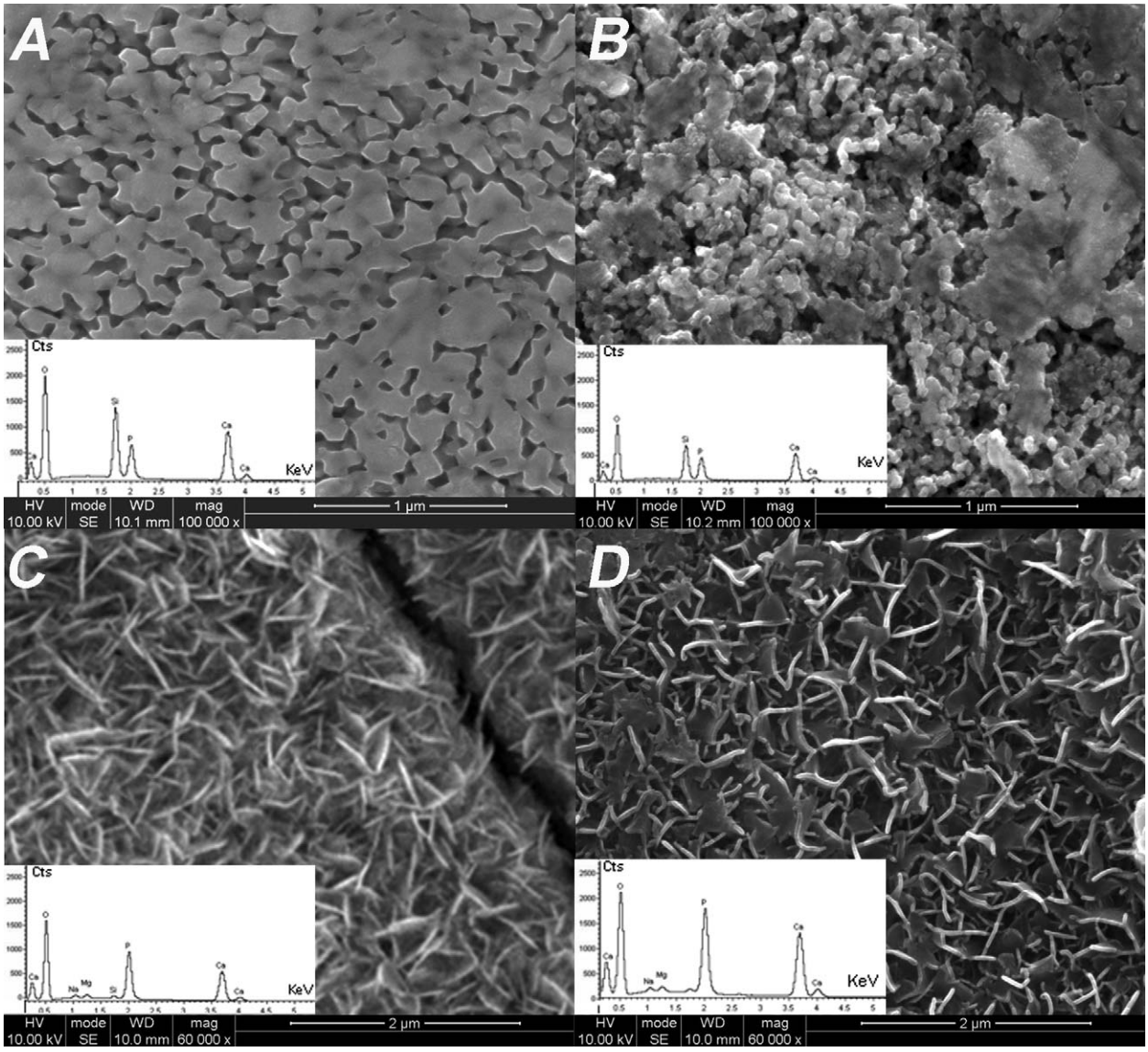

Fig. 7. Scanning electron micrograph of the sample surface of glass-ceramic after exposure to SBF *in vitro* test. (A) 3 days, (B) 7 days, (C) 14 days, (D) 21 days.

the glass ceramic. The lattice parameters ($a = b$ and c) calculated for this phase were slightly higher than the ones reported in the literature for stoichiometric hydroxyapatite and calcium deficient apatite (Table 3). These small differences may be caused by replacement of some [PO_4] groups by [SiO_4] groups in the hydroxyapatite framework, forming a silicate-substituted calcium deficient hydroxyapatite Si-HAdCa ($Ca_9(HPO_4)(PO_4)_{5-y}(SiO_4)_y(OH)_{1-y}\square_y$). The ionic radius of Si^{4+} (0.42 Å) is larger than the one of P^{5+} (0.35 Å), which is in agreement with the observed increase in lattice constants for Si-HAdCa.[34,35]

As determined by SEM/EDS, the material presents a dense and homogeneous microstructure composed of domains of around 2 µm in diameter, formed by a residual amorphous phase that enclosed a mixture of nanosized apatite and wollastonite-2 M crystals (Fig. 3). TEM/EDS analyses confirmed that this nanostructure was formed from ellipsoidal apatite and wollastonite-2 M nanoparticles in the range of about

Table 3
Lattice parameters of pure hydroxyapatite and Ca-deficient apatite as reported in the literature.

	Lattice parameters					
	a	*b*	*c*	alpha	beta	gamma
Hydroxyapatite[33]	9.413	9.413	6.875	90	90	120
Ca-deficient apatite[28]	9.440(1)	9.440(1)	6.879(2)	90	90	120

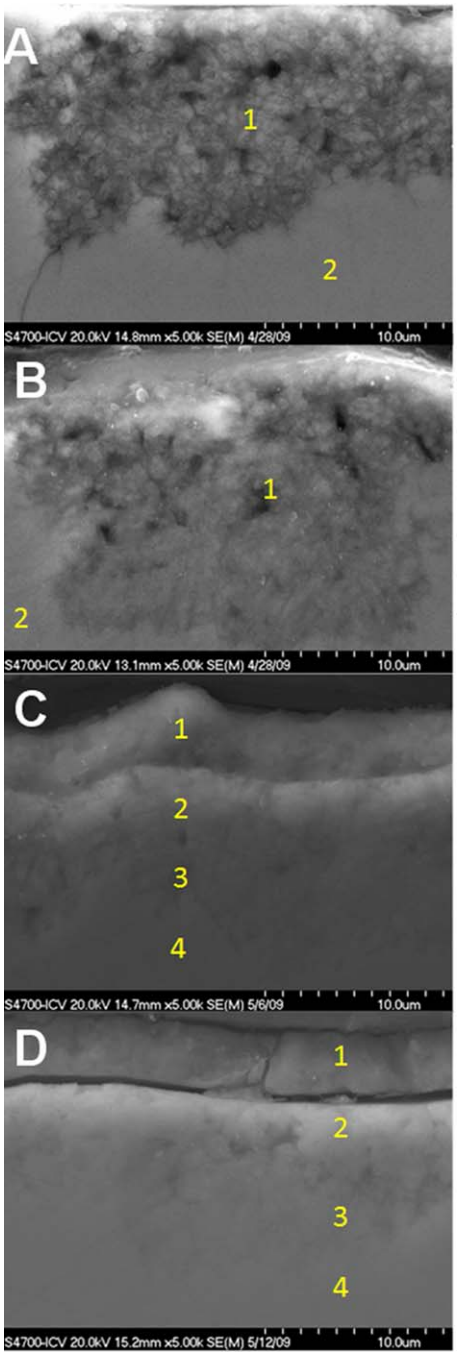

EDS-Microanalysis of Figure A

Zone	Atomic %		
	Si	P	Ca
1	28.90	20.81	50.29
2	31.46	15.23	53.31

EDS-Microanalysis of Figure B

Zone	Atomic %		
	Si	P	Ca
1	27.73	21.53	50.74
2	31.46	15.56	52.98

EDS-Microanalysis of Figure C

Zone	Atomic %		
	Si	P	Ca
1	3.83	36.14	60.03
2	20.98	28.47	50.55
3	24.11	26.80	49.09
4	31.49	15.40	53.11

EDS-Microanalysis of Figure D

Zone	Atomic %		
	Si	P	Ca
1	2.57	36.35	61.08
2	24.75	24.72	50.53
3	29.48	21.17	49.35
4	32.68	16.50	50.82

Fig. 8. Scanning electron micrographs and EDS microanalysis of a cross section of the glass ceramic after soaking in SBF for (A) 3 days, (B) 7 days, (C) 14 days and (D) 21 days.

20–50 nm in length and 20 nm in diameter (Fig. 5). This micro-nanostructure should improve mechanical properties of the material in comparison with the parent glass. The preliminary micro-hardness measurements showed that the micro-hardness (H_V) of the glass-ceramic is $H_V = 6.5 \pm 0.3$ GPa, while a lower value of $H_V = 5.1 \pm 0.4$ GPa was recorded for the parent glass.[36]

4.1. In vitro bioactivity studies

The recorded changes in the concentration of the different ions within the SBF, Fig. 6, showed that during the first stage of immersion the glass released Si and Ca ions. On the other hand, the concentration of silicon was increasing continuously during the *in vitro* experiment reaching 0.79 ± 0.03 mmol after 3 weeks.

It means that the phase or phases that were dissolving contained high content of silicon; therefore these will be the Si-rich residual amorphous phase and/or the wollastonite-2 M. The degradation of both phases led to the formation of a porous reaction layer with residual apatite replacing the original glass ceramic at the surface (Figs. 7A and B and 8A and B). During the second stage of immersion between about 1 and 2

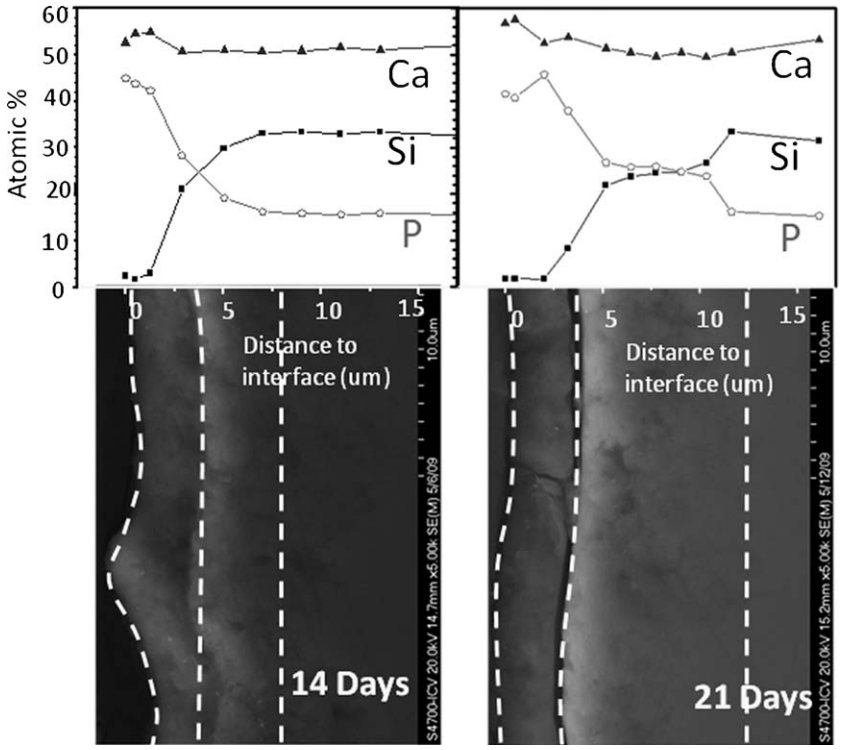

Fig. 9. Scanning electron micrograph and EDS microanalysis of a cross section of the glass-ceramic after soaking in SBF for (A) 14 days and (B) 21 days.

weeks, the concentration of Ca ions in the SBF decreased up to 2.00 ± 0.05 mmol, due to the precipitation of a hydroxy-carbonate apatite layer on the glass ceramic surface (Figs. 7C and D and 8C and D), after which the Ca content remained constant. The phosphorus concentration also decreased up to 0.40 ± 0.05 mmol in the course of 2 weeks, and remained at this level afterwards. This decrease observed between 1 and 2 weeks of exposure to SBF was more prominent due to the formation of the HCA layer. During the first stages of the reaction, the high Ca concentration in the SBF solution, Fig. 6, enhanced the later nucleation of bone like apatite on the surface of the specimen, with high Ca/P ratio ($1.5 \leq Ca/P \leq 1.67$ by EDS). The EDS microanalyses presented in Fig. 7C and D provided data for Ca/P ratio calculations for HCA as a function of soaking time. This information indicated that the new HCA phase was precipitating on the surfaces of the specimens during soaking in the SBF solution. The subsequent changes in the concentration profile observed along the glass ceramic–SBF interface (Fig. 9) indicated that calcium and silicon ions diffused from the bulk glass ceramic to the SBF interface up to a distance of 15 μm, relatively to phosphorus ions. The diffusion process of the ions took place through the pores of the porous reaction layer generated by the degradation of the Si-rich residual amorphous phase and the wollastonite-2 M phase at the glass ceramic/SBF interface (Figs. 8 and 9). This explains why after the 3 week period, the Si content within the SBF was still increasing, Fig. 6.

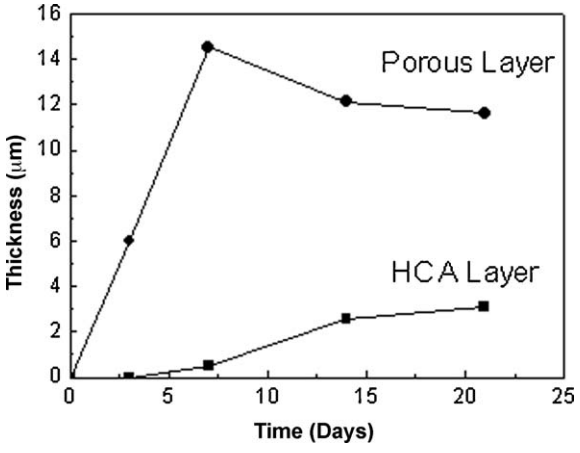

Fig. 10. Evolution of the thickness of the porous reaction layer (with residual apatite from the glass ceramic) as a function of exposure time to SBF. The precipitated HCA layer is also seen.

Basically, the overall reaction can be summarised as follows: the mechanism of the HCA layer formation on the surface of the glass ceramic took place by interdiffusion and chemical reactions of the main components of the SBF (H_3O^+, OH^-– Ca^{2+}, HPO_4^{2-}) and the glass ceramic (Ca^{2+}, $HSiO_3^-$ and HPO_4^{2-}). These processes occurred firstly at the grain boundaries. In case of longer reaction times, the diffusion process occurred intergranular and the open porosity was generated within the material during the first stages of the process (Figs. 7A and B and 8A and B). Once the formation of the HCA layer was established the various ionic species diffused through this layer and the reaction continued (Figs. 8C and D and 9).

The TEM/EDS results were essential in understanding these processes. Fig. 11A shows a high magnification TEM image of the removed reaction product from the glass ceramic sample soaked in SBF for 3 days. Selected area diffraction in Fig. 11B indicated that these particles correspond to the starting material,

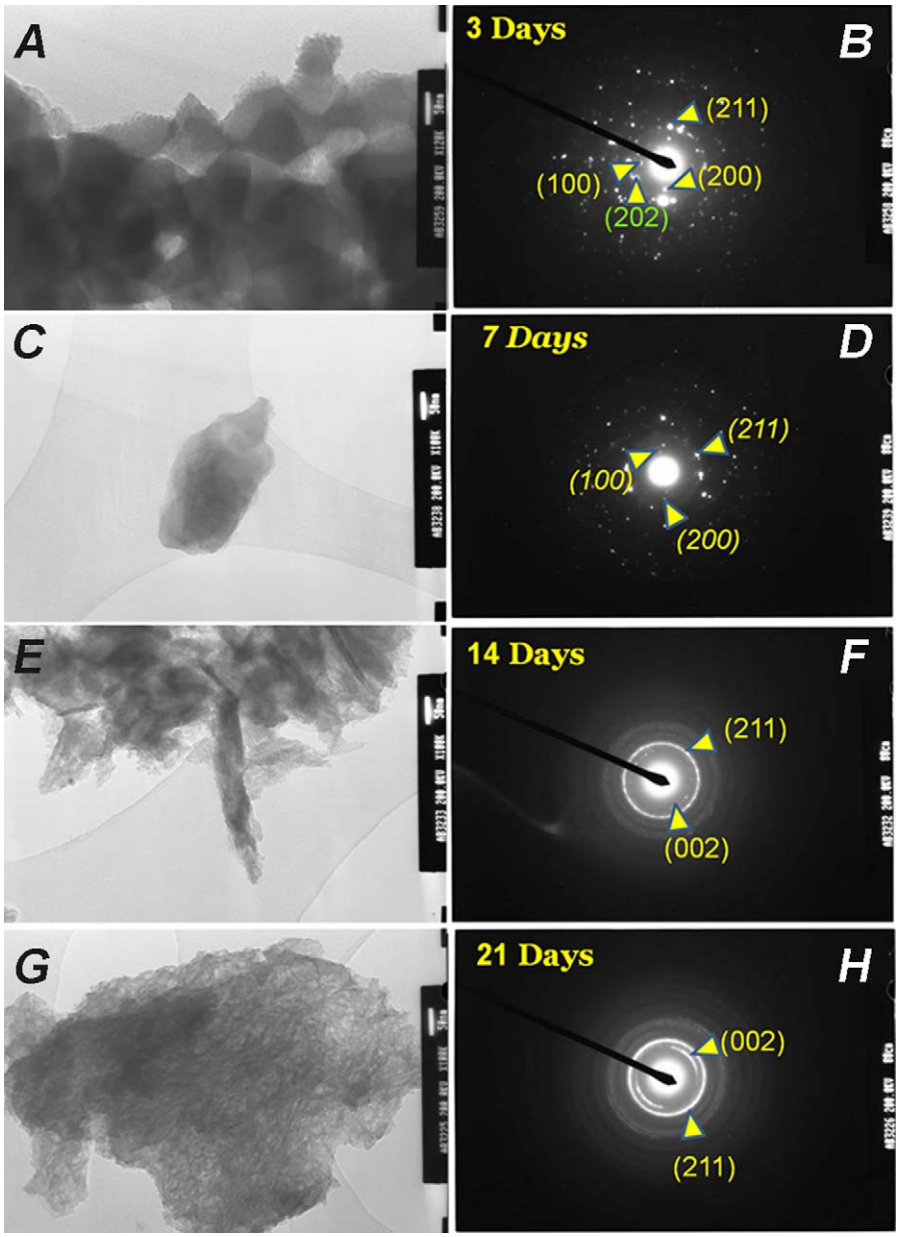

Fig. 11. Transmission electron micrographs and SAD of the surface product from the glass ceramic sample soaked in SBF for different times. (A and B) 3 days, (C and D) 7 days, (E and F) 14 days, (G and H) 21 days.

since some diffraction spots correspond to the wollastonite-2 M. On the other hand, Fig. 11G shows the microstructure of the reaction surface product of the glass ceramic soaked in SBF for 21 days. The equivalent SAD in Fig. 11H clearly indicates on a preferential orientation of the HCA crystals in [0 0 2] direction. This observation agrees with the SEM results presented in Fig. 7D, which demonstrates that the HCA layer contains the interlocked particles of the plate-like morphology. A comparison with the SAD of the removed surface product from the glass ceramic sample soaked in SBF for 14 days in Fig. 11F indicated that the amount of the HCA crystals was significantly smaller than in 21 days sample, because the (0 0 2) arc was less prominent. Overall, these complementary TEM data confirmed that a quantity of a new HCA phase precipitated on the surfaces of the specimens was a function of soaking time in the SBF solution.

On the other hand, the reaction surface product from the glass ceramic sample soaked in SBF for 7 days was partially composed of amorphous silica (Fig. 12). The presence of the amorphous silica layer, as reported in the scientific bibliography for this sort of reactions,[37–39] was not detected by the SEM/EDS studies of the cross sections (Figs. 8 and 9), which indicates that the layer was rather thin or discontinuous and only detectable by TEM, which operates at high resolution level.

When the glass ceramic is placed in contact with physiological fluids, the pH variations are extremely important for its biocompatibility. The pH variations of the SBF (from 7.40 ± 0.02 to 7.50 ± 0.05) during the first 21 days of soak-

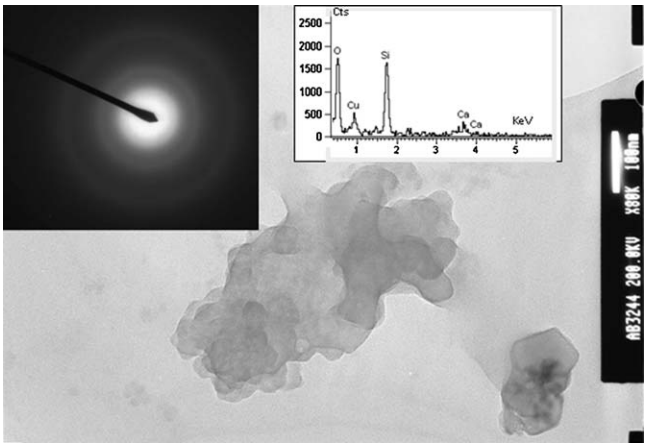

Fig. 12. Transmission electron micrograph and SAD of the surface product from the glass ceramic sample surfaces soaked in SBF for 7 days.

ing are not significant. As reported elsewhere, at this pH range the more stable calcium phosphate hydrate gave rise to calcium deficient apatite ($Ca_{10-x}(HPO_4)_x(PO_4)_{6-x}(OH)_{2-x}$ $(0<x<1)$ Ca/P = 1.5–1.67, pH 6.5–9.5).[40]

It is known that osteoblasts prefer moderately alkaline conditions (pH 7.5–8.0), and changes in pH could cause severe damage to cells' viability.[41–43] However, the pH values recorded for the glass ceramic was favorable. This was confirmed by experiments carried out on cell cultures using human bone marrow stem cells.[36]

The results of this study showed that the mechanism of interfacial reaction between bioeutectic glass ceramic and SBF is in agreement with the surface reaction stages proposed by Cao and Hench[44], specifically with the first five steps that involve surface dissolution and precipitation. The remaining stages described by these researchers[44] involve cells activity. The bioactive process of the material developed in the present research starts with two simultaneous reactions (a) and (b); and can be described as follows:

(a) The SBF in contact with the glass ceramic reacts dissolving the amorphous phase of the material:

$$\text{Amorphous phase}_{(s)} + H_2O_{(aq.)} \rightarrow Ca^{2+}{}_{(aq.)} + HSiO_3{}^{-}{}_{(aq.)} + HPO_4{}^{2-}{}_{(aq.)} + OH^{-}{}_{(aq.)} \quad (2)$$

(b) The wollastonite-2 M phase in contact with the SBF starts to react via an ionic exchange of H^+ and OH^- from the SBF for Ca^{2+} and silicate anions from the wollastonite-2 M network according to the following reactions:

$$CaSiO_3(2\,M)_{(s)} + H^{+}{}_{(aq.)} \rightarrow HSiO_3{}^{-}{}_{(aq.)} + Ca^{2+}{}_{(aq.)} \quad (3)$$

($\Delta G_{37\,^\circ C} = -5.332$ kcal; equilibrium constant at 37 °C $K = 5.718E^{+3}$; $\log K = 3.757$)

$$CaSiO_3(2\,M)_{(s)} + OH^{-}{}_{(aq.)} \rightarrow Ca^{2+}{}_{(aq.)} + SiO_3(OH)^{3-}{}_{(aq.)} \quad (4)$$

($\Delta G_{37\,^\circ C} = 7.843$ kcal; equilibrium constant K at 37 °C $K = 2.969E^{-6}$; $\log K = -5.527$)

$$CaSiO_3(2\,M)_{(s)} + H_2O_{(aq.)} \rightarrow Ca^{2+}{}_{(aq.)} + HSiO_3{}^{-}{}_{(aq.)} + OH^{-}{}_{(aq.)} \quad (5)$$

($\Delta G_{37\,^\circ C} = 13.997$ kcal; equilibrium constant K at 37 °C $K = 1.368E^{-10}$; $\log K = -9.864$)

$$CaSiO_3(2\,M)_{(s)} + H_2O_{(aq.)} \rightarrow Ca^{2+}{}_{(aq.)} + SiO_4{}^{4-}{}_{(aq.)} + 2H^{+}{}_{(aq.)} \quad (6)$$

($\Delta G_{37\,^\circ C} = 50.154$ kcal; equilibrium constant at 37 °C $K = 4.523E^{-36}$; $\log K = -35.345$)

The silicate anions can be produced according to reactions (3) to (6). Reaction (3) has the lowest Gibbs free energy and therefore is the most viable. According to the values of the constant equilibrium the viability of the reactions will follow the following order (3) > (4) > (5) > (6), being $HSiO_3{}^{-}$ (aq.) and Ca^{2+} (aq.) the major ions.

(c) With the release of the calcium and phosphorous ions from the wollastonite-2 M and the amorphous phase, many Si–OH groups are formed on the surfaces of the glass ceramic forming an amorphous silica rich phase. These silanol groups could induce heterogeneous nucleation of apatite. When the ionic activities in the SBF at the neighbourhood of the reacting surface reach the solubility of the carbonated apatites, this phase starts to precipitate onto the glass ceramic surface, this process takes less than 7 days, following this reaction:

$$(6-x)\,HPO_4{}^{2-}{}_{(aq.)} + xCO_3{}^{2-}{}_{(aq.)} + 10-x/2Ca^{2+}{}_{(aq.)} + (8+x)OH^{-}{}_{(aq.)} \rightarrow Ca_{10-x/2}(PO_4)_{6-x}(CO_3)_x(OH)_{2(s)} + 6H_2O_{(aq.)} \quad (7)$$

For charge balance $CO_3{}^{2-}$ ions substituting $PO_4{}^{3-}$ yield the loss of Ca^{2+} ions.

(d) Once apatite nuclei are formed on the surface of the porous layer, they can grow spontaneously by consuming calcium and phosphate ions from the surrounding SBF solution.

A simulation of the solubility process by thermodynamic function reported in the literature[45] established the solubility sequence of wollastonite-2 M ≫ apatite in SBF, matching the experimental results from this study.

The results showed that the morphology generated in the simulated physiological media was controlled by different phases' solubility which generated changes of the surface chemistry and the surface topography. This mechanism leads to the "*in situ*" formation of a porous interconnected structure of apatite, which could be expected to promote the bone growth when the material is implanted into bone defects. The phases with highest solubility rates (amorphous phase > wollastonite-2M ≫ apatite) control the rate of HCA layer formation on the surface of the glass ceramic material.

5. Conclusions

A glass ceramic composed of apatite, wollastonite-2 M and an amorphous phase (44.8; 28.0 and 27.2 wt%, respectively) was manufactured by a specific thermal cycle that allows the devitrification process of the $Ca_3(PO_4)_2$–$CaSiO_3$ binary system's stoichiometric eutectic composition.

The glass ceramic exposed to the SBF releases predominantly Ca and Si ions, due to the dissolution of the amorphous phases and wollastonite-2 M, leading to the formation of an apatite-like layer onto the surface of the material. This layer reached about 4 μm of thickness in less than 21 days.

The results evidenced that microstructure and morphology generated in the simulated physiological media was controlled by different solubility rates of the phases. This mechanism leads to the "*in situ*" formation of an interconnected porous structure of residual apatite, which is expected to promote the bone ingrowths. The phases with the highest solubility rate like amorphous phase and wollastonite-2 M control the newly formed HCA layer on the surface of the glass ceramic.

This apatite–wollastonite 2 M glass-ceramics could serve as a promising platform for regeneration of hard tissue.

Acknowledgements

This work was supported by Science and Technology Inter-Ministry Commission of Spain under projects CICYT MAT2006-12749-C02-01-02 & MAT2010-17753. M. Magallanes-Perdomo wishes to acknowledge financial support (AP 2005 - 5181) from the Ministry of Science and Innovation of Spain.

References

1. Best SM, Porter AE, Thian ES, Huan J. Bioceramics: past, present and for the future. *J Eur Ceram Soc* 2008;**28**:1319–27.
2. Chevalier J, Gremillard L. Ceramics for medical applications: a picture for the next 20 years. *J Eur Ceram Soc* 2009;**29**:1245–55.
3. Dorozhkin SV. Bioceramics of calcium orthophosphates. *Biomaterials* 2010;**31**:1465–85.
4. Ni S, Chang J, Chou L. A. novel bioactive porous $CaSiO_3$ scaffold for bone tissue engineering. *J Biomed Mater Res A* 2006;**76**:196–205.
5. Carlisle EM. Biochemical and morphological changes associated with long bone abnormalities in silicon deficiency. *J Nutr* 1980;**110**:1046–55.
6. Carlisle EM. A silicon requirement for normal skull formation. *J Nutr* 1980;**10**:352–9.
7. Porter AE. Nanoscale characterization of the interface between bone and hydroxyapatite implants and the effect of silicon on bone apposition. *Micron* 2006;**37**:681–8.
8. Pietak AM, Reid JW, Stott MJ, Sayer M. Silicon substitution in the calcium phosphate bioceramics. *Biomaterials* 2007;**28**:4023–32.
9. Liu X, Morra M, Carpi A, Li B. Bioactive calcium silicate ceramics and coatings. *Biomed Pharmacother* 2008;**62**:526–9.
10. Iimori Y, Kameshima Y, Okada K, Hayashi S. Comparative study of apatite formation on $CaSiO_3$ ceramics in simulated body fluids with different carbonate concentrations. *J Mater Sci Mater Med* 2005;**16**(1):73–9.
11. El-Ghannam A, Ducheyne P, Shapiro IM. Porous bioactive glass and hydroxyapatite ceramic affect bone cell function *in vitro* along different time lines. *J Biomed Mater Res* 1997;**36**:167–80.
12. Kokubo T, Kim H-M, Kawashita M. Novel bioactive materials with different mechanical properties. *Biomaterials* 2003;**24**:2161–75.
13. Kokubo T, Shigematsu M, Nagashima Y, Tashiro M, Nakamura T, Yamamuro T, et al. Apatite- and wollastonite-containing glass ceramics for prosthetic applications. *Bull Inst Chem Res Kyoto Univ* 1982;**60**:260–8.
14. Salinas AJ, Roman J, Vallet-Regi M, Oliveira JM, Correia RN, Fernandes MH. *In vitro* bioactivity of glass and glass-ceramics of the $3CaO{\cdot}P_2O_5$–$CaO{\cdot}SiO_2$–$CaO{\cdot}MgO{\cdot}2SiO_2$ system. *Biomaterials* 2000;**21**:251–7.
15. Liu D-M, Chou H-M. Formation of a new bioactive glass-ceramic. *J Mater Sci: Mater Med* 1994;**5**:7–10.
16. Magallanes-Perdomo M, Carrodeguas RG, Pena P, De Aza PN, De Aza S, De Aza AH. Non-isothermal devitrification study of wollastonite-tricalcium phosphate Bioeutectic® glass. *Key Eng Mater* 2009;**396–398**:127–30.
17. Magallanes-Perdomo M, Pena P, De Aza PN, Carrodeguas RG, Rodriguez MA, Turrillas X, et al. Devitrification studies of wollastonite–tricalcium phosphate eutectic glass. *Acta Biomater* 2009;**5**:3057–66.
18. De Aza PN, Guitián F, De Aza S. Phase-diagram of wollastonite-tricalcium phosphate. *J Am Ceram Soc* 1995;**78**:1653–6.
19. De La Torre AG, Bruque S, Aranda MAG. Rietveld quantitative amorphous content analysis. *J Appl Crystallogr* 2001;**34**:196–202.
20. Larson AC, Von Dreele RB. Los Alamos National Laboratory Report No. LA-UR-86-748. Los Alamos National Laboratory, Los Alamos, NM, 1994. GSAS program at http://www.ncnr.nist.gov/programs/crystallography/software/gsas.html.
21. Kokubo T, Takadama H. How useful is SBF in predicting in vivo bone bioactivity? *Biomaterials* 2006;**27**:2907–15.
22. HSC Chemistry® for Windows, v 5.1. Outokumpu Research on Information Service, Pori, Finland.
23. Navarro JF. *El Vidrio (The Glass)*. 3rd ed. Spain: Consejo Superior de Investigationes Científicas (CSIC); 2003. p. 270 [in Spanish].
24. Varshneya AK. *Fundamentals of inorganic glasses*. 2nd ed. Sheffield: Society of Glass Technology; 2006. p. 682.
25. Vogel W. *Chemistry of glass*. Ohio: The American Ceramic Society; 1985. p. 325.
26. Aguiar H, Solla EL, Serra J, Gonzalez P, Leon B, Almeida N, et al. Orthophosphate nanostructures in SiO_2–P_2O_5–CaO–Na_2O–MgO bioactive glasses. *J Non-Cryst Solids* 2008;**354**:4075–80.
27. Wilson RM, Elliott JC, Dowker SE, Rodriguez-Lorenzo LM. Rietveld refinements and spectroscopic studies of the structure of Ca-deficient apatite. *Biomaterials* 2005;**26**:1317–27.
28. Wilson RM, Elliott JC, Dowker SE, Rodriguez-Lorenzo LM. Ca9.303(PO4)6(OH)0.6061.97(H2O). Inorganic Crystal Structure Database, ICSD Collection Code: 152190.
29. Trojer FJ. The crystal structure of parawollastonite. *Zeitschrift Fur Kristallographie Kristallgeometrie Kristallphysik Kristallchemie* 1968;**127**:291–308.
30. Trojer FJ. $CaSiO_3$–wollastonite-2 M. Inorganic Crystal Structure Database, ICSD Collection Code: 34908.
31. Young RA. *The Rietveld method*. Oxford: University Press; 1993. p. 336.
32. Deer WA, Howie RA, Zussman J. *Rock-forming minerals. Vol 2. Single-chain silicates: non-pyroxenes*. Oxford: Geological Society; 2001. p. 547–563.
33. Kay MI, Young RA, Posner AS. Crystal structure of hydroxyapatite. *Nature* 1964;**204**:1050–2.
34. Kim SR, Lee JH, Kim YT, Riu DH, Jung SJ, Lee YJ, et al. Synthesis of Si Mg substituted hydroxyapatites and their sintering behaviors. *Biomaterials* 2003;**24**:1389–98.
35. Tian T, Jiang D, Zhang J, Lin Q. Synthesis of Si-substituted hydroxyapatite by wet mechanochemical method. *Mater Sci Eng* 2008;**C28**:57–63.
36. Magallanes-Perdomo M, Mateus AY, De Aza AH, Texeira S, Monteiro FJ, De Aza S, et al. *In vitro* study of the proliferation and growth of human bone marrow cells on apatite–wollastonite 2 M glass-ceramics. *Acta Biomater* 2010;**6**:2254–63.
37. Kokubo T, Kushitani H, Ohtsuki C, Sakka S. Chemical reaction of bioactive glass and glass-ceramics with a simulated body fluid. *J Mater Sci Mater Med* 1992;**3**:79–83.
38. De Aza PN, Fernandez-Pradas JM, Serra P. *In vitro* bioactivity of laser ablation pseudowollastonite coating. *Biomaterials* 2004;**25**:1983–90.

39. Aguiar H, Solla EL, Serra J, Gonzalez P, Leon B, Malz F, et al. Raman and NMR study of bioactive Na_2O–MgO–CaO–P_2O_5–SiO_2 glasses. *J Non-Cryst Solids* 2008;**354**:5004–8.
40. Sergey V, Dorozhkin. Calcium orthophosphate cements for biomedical application. *J Mater Sci* 2008;**43**:3028–57.
41. Ramp WK, Lenz LG, Kaysinger KK. Medium pH modulates-matrix, mineral and energy metabolism in cultured chick bones and osteoblast-like cells. *Bone Miner* 1994;**24**:59–73.
42. Kaysinger KK, Ramp WK. Extracellular pH modulates the activity of cultured human osteoblasts. *J Cell Biochem* 1998;**68**:83–9.
43. El-Ghannam A, Ducheyne P, Shapiro J. Formation of surface reaction products on bioactive glass and their effects on the expression of the osteoblastic phenotype and the deposition of mineralized extracellular matrix. *Biomaterials* 1997;**18**:295–303.
44. Cao W, Hench LL. Bioactive materials. *Ceram Int* 1996;**22**:493–507.
45. Sainz MA, Pena P, Serena S, Caballero A. Influence of design on bioactivity of novel $CaSiO_3$-$CaMg(SiO_3)_2$ bioceramics: *in vitro* simulated body fluid test and thermodynamic simulation. *Acta Biomater* 2010;**6**:2797–807.